Drivers and reversibility of abrupt ocean state transitions in the Amundsen Sea, Antarctica

Justine Caillet[1], Nicolas C Jourdain[1], Pierre Mathiot[1], Hartmut H Hellmer[2], and Jérémie Mouginot[1]

[1]Univ. Grenoble Alpes
[2]Alfred Wegener Institute Helmholtz Centre for Polar and Marine Research

November 22, 2022

Abstract

Ocean warming around Antarctica has the potential to trigger marine ice-sheet instabilities. It has been suggested that abrupt and irreversible cold-to-warm ocean tipping points may exist, with possible domino effect from ocean to ice-sheet tipping points. A 1/4° ocean model configuration of the Amundsen Sea sector is used to investigate the existence of ocean tipping points, their drivers, and their potential impact on ice-shelf basal melting. We apply idealized atmospheric perturbations of either heat, freshwater or momentum fluxes, and we characterize the key physical processes at play in warm-to-cold and cold-to-warm climate transitions. Relatively weak perturbations of any of these fluxes are able to switch the Amundsen Sea to an intermittent or permanent cold state, i.e., with ocean temperatures close to the surface freezing point and very low ice-shelf melt rate. The transitions are reversible, i.e., cancelling the atmospheric perturbation brings the ocean system back to its unperturbed state within a few decades. All the transitions are primarily driven by changes in surface buoyancy fluxes over the continental shelf, as a direct consequence of the freshwater flux perturbation, or through changes in net sea-ice production resulting from either heat flux perturbations or from changes in sea-ice advection for the momentum flux perturbation. These changes affect the vertical ocean stratification and thereby ice-shelf basal melting. For warmer climate conditions than presently, the surface buoyancy forcing becomes less important as there is a decoupling between the surface and subsurface layers, and ice-shelf melt rates appear less sensitive to climate conditions.

Drivers and reversibility of abrupt ocean state transitions in the Amundsen Sea, Antarctica

Justine Caillet[1], Nicolas C. Jourdain[1], Pierre Mathiot[1], Hartmut H. Hellmer[2], Jérémie Mouginot[1]

[1]Univ. Grenoble Alpes, CNRS, IRD, Grenoble INP, IGE, 38000 Grenoble, France
[2]Alfred Wegener Institute Helmholtz Centre for Polar and Marine Research, Bremerhaven, Germany

Key Points:

- The currently warm ice-shelf cavities of the Amundsen sector could become or have been cold for slightly colder climatic conditions.
- The transitions are reversible:cancelling the atmospheric perturbation brings the ocean back to its unperturbed state within a few decades.
- All the transitions are primarily driven, at multi-decadal scale, by changes in surface buoyancy fluxes over the continental shelf.

Corresponding author: Justine CAILLET, justine.caillet@univ-grenoble-alpes.fr

Abstract

Ocean warming around Antarctica has the potential to trigger marine ice-sheet instabilities. It has been suggested that abrupt and irreversible cold-to-warm ocean tipping points may exist, with possible domino effect from ocean to ice-sheet tipping points. A 1/4° ocean model configuration of the Amundsen Sea sector is used to investigate the existence of ocean tipping points, their drivers, and their potential impact on ice-shelf basal melting. We apply idealized atmospheric perturbations of either heat, freshwater or momentum fluxes, and we characterize the key physical processes at play in warm-to-cold and cold-to-warm climate transitions. Relatively weak perturbations of any of these fluxes are able to switch the Amundsen Sea to an intermittent or permanent cold state, i.e., with ocean temperatures close to the surface freezing point and very low ice-shelf melt rate. The transitions are reversible, i.e., cancelling the atmospheric perturbation brings the ocean system back to its unperturbed state within a few decades. All the transitions are primarily driven by changes in surface buoyancy fluxes over the continental shelf, as a direct consequence of the freshwater flux perturbation, or through changes in net sea-ice production resulting from either heat flux perturbations or from changes in sea-ice advection for the momentum flux perturbation. These changes affect the vertical ocean stratification and thereby ice-shelf basal melting. For warmer climate conditions than presently, the surface buoyancy forcing becomes less important as there is a decoupling between the surface and subsurface layers, and ice-shelf melt rates appear less sensitive to climate conditions.

Plain Language Summary

The West Antarctic Ice Sheet is under the threat of a partial collapse, which would induce rapid global sea level rise. This threat is partly related to the thinning of floating ice shelves, and the consequent retreat of the grounding line, which is a self-sustained ice dynamics process. It is triggered by increased basal melting of the ice shelves, which results from enhanced flow of relatively warm waters onto the continental shelf. It has been suggested that self-sustained ocean processes may lead to abrupt changes in the flow of warm water into ice-shelf cavities, which could facilitate the tipping to a marine ice-sheet instability. Here, we analyze whether such abrupt ocean changes can occur under cold-to-warm or warm-to-cold transitions in the Amundsen Sea, West Antarctica. We use a regional ocean model with a set of idealized local atmospheric perturbations to characterize the thresholds and reversibility of ocean abrupt changes. We find that the currently warm Amundsen Sea could switch intermittently or permanently to a cold state for relatively weak atmospheric perturbations and could be slightly warmer in the future. All transitions are reversible. The main mechanism involved on decadal scale is related to a change in the surface buoyancy fluxes.

1 Introduction

The West Antarctic Ice Sheet has lost mass over the last few decades and has thus contributed significantly to global sea level rise. Warming of the oceanic sub-surface seems to have caused an increase in melting under floating ice shelves, particularly in the Amundsen Sea (Jenkins et al., 2018). Depending on the bedrock slope direction (Schoof, 2007; Pattyn et al., 2012) and ice-shelf lateral buttressing (Gudmundsson, 2013), a sufficiently strong and persistent increase in basal melting can lead to a Marine Ice-Sheet Instability (MISI), resulting in a self-sustained retreat of the glacier's grounding line and to the acceleration of its flow (Favier et al., 2014; Joughin et al., 2014).

Instabilities are triggered above a certain oceanic warming (critical threshold or tipping point), with the possible existence of multiple thresholds. Thus, Rosier et al. (2021) estimated that Pine Island Glacier would undergo a MISI and major mass loss for an oceanic warming of +1.2°C relative to the present. Garbe et al. (2020) estimated that a tipping point of +2°C global warming relative to pre-industrial could cause a MISI of the entire West Antarctic Ice Sheet. Tipping points are characterized by a hysteresis, i.e., restoring the forcing to before the occurrence of the tipping point is not sufficient to restore the system to its original state. Identifying these tipping points precisely and linking them to climate projections would allow the effects of future rapid sea level rise to be anticipated and possibly mitigated (Hinkel et al., 2019).

The abrupt nature of these ice tipping points in West Antarctica could be enhanced if ocean warming itself is subject to a tipping point. This would be a cascading tipping point, or domino effect (Dekker et al., 2018; Brovkin et al., 2021; Wunderling et al., 2021). It has been suggested, that beyond a certain threshold of melting, the Greenland Ice Sheet could induce a sudden weakening of the Atlantic Meridional Overturning Circulation, which, in turn, would lead to ocean warming around Antarctica (Turney et al., 2020; Wunderling et al., 2021).

Another type of oceanic tipping point has been highlighted in the Weddell Sea (Hellmer et al., 2012, 2017). Reduced sea-ice formation under continued global warming, a freshening of the continental shelf, and increased ocean surface stress could cause the slope current to diverge in the southeast Weddell Sea. The reorientation would facilitate the entry of Warm Deep Water, a cooler variant of Circumpolar Deep Water (CDW), onto the continental shelf and significantly increase basal melting, which would lead to a self-reinforcing process due to the injection of meltwater. The process is irreversible with the twentieth-century atmospheric forcing: only an imposed decrease in basal melt rate can hinder the self-sustaining process.

The Amundsen Sea environment is very different as relatively warm cavities already exist (Jacobs et al., 1996, 2012). Paleoclimatic indicators suggest that the entire Amundsen continental shelf was covered by an ice sheet (either resting or floating) at the Last Glacial Maximum (Larter et al., 2014). A particularly large retreat of the ice-sheet front and grounding line occurred between 20,000 and 10,000 years BP (Larter et al., 2014), with further smaller retreats occurring thereafter, notably around 1945 and then 1970 (Smith et al., 2017). Ocean temperatures and warming rates during these transitions are not known, but it is possible that oceanic tipping points similar to those reported by Hellmer et al. (2012, 2017) for the Weddell Sea occurred in the Amundsen Sea area as well.

In this paper, we analyze under which atmospheric forcing conditions warm-to-cold, cold-to-warm and warm-to-warmer ocean transitions in the Amundsen Sea have occurred or could occur, and we test the reversibility of these transitions, i.e., the presence of hysteresis. We use a regional ocean modelling approach with a set of idealized atmospheric perturbations.

2 Materials and Methods

2.1 Model and configuration

The Nucleus for European Modelling of the Ocean (NEMO) model, version 3.6, including the OPA ocean model (Madec & the NEMO Team, 2016) and the Louvain-la-Neuve sea-ice model LIM-3.6 (Rousset et al., 2015), is used in a regional configuration of the Amundsen Sea (Fig. 1). Our model parameters are similar to Jourdain et al. (2019), with a representation of ice–ocean exchange beneath static ice shelves, with melt rate depending on ocean velocity, temperature and salinity (Mathiot et al., 2017; Jourdain et al., 2017), and barotropic tides prescribed as lateral boundary conditions from seven constituents of the FES2012 tidal model (Carrère et al., 2012; Lyard et al., 2006).

Compared to Jourdain et al. (2019), the domain is slightly extended, now covering from 142°W to 85°W and from 76.3°S to 59.8°S, and the resolution is reduced to 1/4° in longitude, i.e., a quasi-isotropic resolution ranging from 14 km at the northern bound-

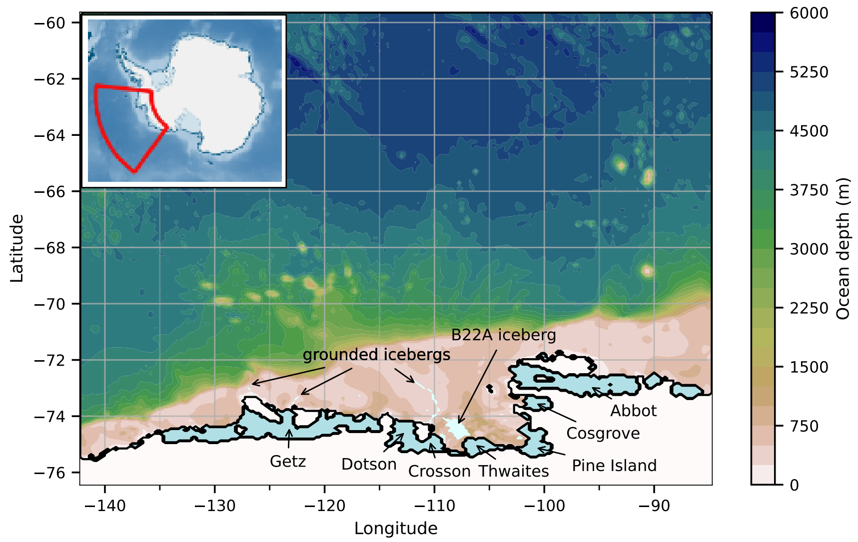

Figure 1. Used regional configuration of the Amundsen Sea. Bathymetry and ice-shelf draft are from the second version of the BedMachine Antarctica dataset (Morlighem et al., 2020). Grounded ice is shaded in white, ice shelves are colored in blue and main tabular icebergs in light cyan. The general view is drawn from the geospatial data package Quantarctica (Matsuoka et al., 2021).

ary to 6.5 km in the southernmost part of the domain. Bathymetry, as well as surface and lateral boundary conditions also differ from Jourdain et al. (2019) and cover the period 1958-2018 in this study. The period 1958-1968 is left for spin-up and discarded in our analyses.

The bathymetry and ice-shelf draft interpolated on the model grid are from the second version of the BedMachine Antarctica dataset (Morlighem et al., 2020). This recent dataset represents Thwaites Ice Shelf after its partial collapse. The B22A iceberg as well as other very large tabular icebergs, absent from BedMachine Antarctica, are represented as static flat ice shelves in the middle of the ocean (assumed to be grounded by the subgrid-scale bathymmetry when no grounded area is explicitly represented). Their shape and location are derived from a MODIS-visible image (provided by the US National Snow and Ice Data Center) taken on 5th September 2003. The huge B22A iceberg calved from the Thwaites ice tongue in 2002 and has drifted very slowly since then (Antarctic Iceberg Tracking Database, Budge & Long, 2018). A similar calving event occurred in the late 1960s (Lindsey, 1995). The resulting iceberg was eventually designated B10 in 1992 when it started a 15-year drift across the Amundsen Sea before breaking up and drifting further away (Budge & Long, 2018). Numerous smaller icebergs regularly drift westward in the Amundsen Sea and ground on the eastern flank of bathymetric ridges shallower than approximately 400 m (Mazur et al., 2017). We therefore artificially place a wall along the 380 m isobath on the eastern flank of Bear Ridge (in a similar way as Bett et al., 2020), north of Siple Island, and on the main ridge in between. These permanent lines of grounded icebergs were shown to favor the formation of polynyas with impact on ice-shelf melting (Nakayama et al., 2014; Bett et al., 2020).

The conditions at the lateral ocean and sea-ice boundaries are derived from the 5-day mean outputs of a global simulation very similar to the one described in Merino et al. (2018) except that it is spun up from 1958 and that the imposed ice-shelf melt flux increases linearly from 1990 to 2005 and is constant before and after that, with values corresponding to the FRESH+ and FRESH− reconstructions of Merino et al. (2018). Here, the temperature and salinity boundary conditions are corrected by the difference between the seasonal climatology of the World Ocean Atlas 2018 (WOA18) database (Garcia et al., 2019) and the seasonal climatology of the global simulation. The global simulation used for boundary conditions represents melting of Lagrangian icebergs (Merino et al., 2016), and the corresponding 5-day mean melt fluxes are applied as a freshwater flux at the surface of our regional configuration. The atmospheric forcing data are taken from the JRA55-do reanalysis (Tsujino et al., 2018) between 1958 and 2018. The fluxes between ocean (or sea ice) and atmosphere are calculated using the CORE bulk formulae described in Griffies et al. (2009); Large and Yeager (2004).

Some model parameters are varied to reduce biases in the reference configuration (see Supporting Information), while atmospheric forcing fields are perturbed (Section 2.2) to investigate ocean tipping points.

2.2 Atmospheric forcing perturbations

In the following, we investigate three pathways to induce ocean tipping points in the Amundsen Sea through surface flux modifications of either heat, freshwater, or momentum. We decided to consider idealized atmospheric perturbations in order to identify and isolate the processes at play. Thus, each surface flux is perturbed independently.

The heat flux is perturbed through air temperature, to which the flux is particularly sensitive. To limit the impact of this perturbation on evaporation, and thus on the freshwater flux, specific humidity is also modified consistently with the air temperature perturbation, according to the Clausius Clapeyron law. The choice of air temperature is convenient for the definition of the perturbation range, which is bounded by typical conditions of the Last Glacial Maximum, i.e., approximately -10°C relative to the current temperature (Masson-Delmotte et al., 2010) and by typical projections at 2300 under the SSP5-8.5 scenario, i.e., about 10°C warmer than the current situation (Lee et al., 2021).

For the freshwater flux, we decide to modify precipitation while maintaining the ratio between solid and liquid precipitation for the sake of simplicity (the heat flux associated with snow melting in the ocean is relatively low). Precipitation near Antarctica has been shown to evolve following the Clausius-Clapeyron law (Ligtenberg et al., 2013; Donat-Magnin et al., 2021). The range of variation is therefore indexed to the temperature range considered for the heat flux: precipitation is multiplied by factors between 0.48 and 1.99, corresponding to coldest (-10°C) and warmest (+10°C) climatic conditions, respectively.

The momentum flux is perturbed through meridional shifting of winds. To maintain flux independence, only the wind involved in the momentum flux calculation (i.e., ocean and sea ice surface friction) is modified, while we keep the wind seen by latent and sensible heat fluxes unchanged in the bulk formulae. The applied wind shift ranges between a 4.7° northward shift for coldest (-10°C) climatic conditions (Gray et al., 2021) and a 4.7° southward shift for warmest (+10°C) conditions (extrapolated from the 2100 CMIP5-RCP8.5 sensitivity described in Spence et al., 2014).

For the three types of perturbations, we conduct simulations with intermediate perturbations between the coldest and warmest climate perturbations in order to better characterize potential tipping points. Perturbations are local, only applied on continental shelf and slope. We do not perturb lateral boundary conditions, i.e., we maintain the presence of CDW in front of the continental shelf in all our simulations. It seems clear that cold conditions would prevail if CDW stopped to exist, and it is more interesting to identify how warm-to-cold abrupt transitions could occur in the presence of CDW.

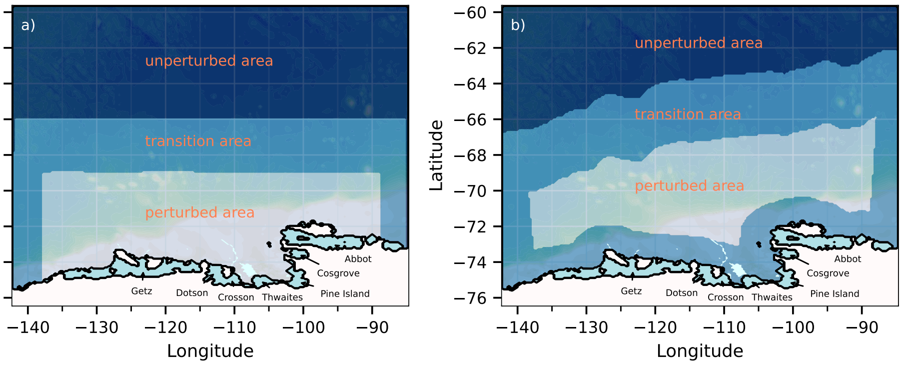

Figure 2. Location of the perturbed area (a) for heat and freshwater fluxes and (b) for momentum flux. The perturbed area is highlighted in light blue, the transition area in blue and the unperturbed area in dark blue. The transition area avoids the artificial formation of strong density gradient or wind curl.

Basal melting highly depends on whether the perturbation is applied only on the continental shelf or on the continental shelf and slope (not shown). We decided to include the continental slope in the perturbed area as this area is relevant for CDW intruding onto the shelf. The ice shelf melt rates are not sensitive to further northward extension of the perturbation area, which indicates some robustness of our methodology. For the heat and freshwater flux perturbations, a transition area of 3° in latitude (about 340 km) and 4° in longitude limits the temperature and precipitation gradient, and thus the formation of strong density gradients, between the perturbed and unperturbed areas (Fig. 2a). For the momentum flux perturbation, we additionally put a coastal transition area of 150 km width between the perturbed wind and the katabatic winds near the ice-sheet edges to avoid creating a substantial artificial wind curl perturbation (Fig. 2b).

2.3 Simulations

In order to assess the model response to atmospheric perturbations, we run a 61-year simulation over the period 1958-2018. The simulation length is a compromise between computational cost and the description of the natural decadal variability of the ocean system, which can potentially impact the system stability and the occurrence of tipping points. The reference experiment corresponds to the configuration retained after calibration (see Supporting Information) with natural atmospheric and oceanic forcing over the modelled period. The model calibration improves the fidelity of the reference simulation although the interannual variability is smaller than expected (consequences will be discussed in section 4). The model spin-up is achieved after 10 years, thus, only the period 1968-2018 is analyzed. The perturbed runs are identical to the reference run except for the atmospheric forcing. We study three possible types of transition: cold-to-warm transitions as reported by Hellmer et al. (2012, 2017) for the Weddell Sea, warm-to-cold and warm-to-warmer transitions related to ancient or distant future climate transitions. When an abrupt ocean transition occurs, reversibility is studied, i.e., for cold-to-warm (C2 in Fig. 3) and warm-to-cold transitions (C3 in Fig. 3).

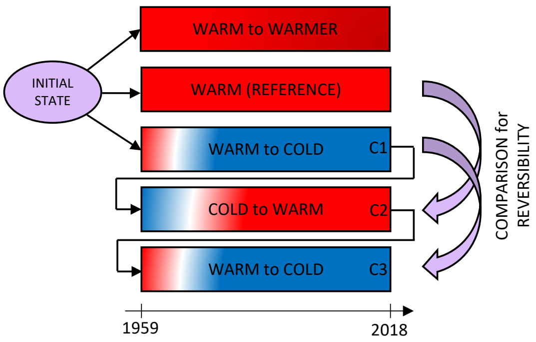

Figure 3. Simulation set-up. The annotations C1, C2 and C3 correspond to the 1^{st}, 2^{nd} and 3^{rd} simulation cycle, respectively. The warm-to-warmer, warm-to-cold (C1) and cold-to-warm simulations enable us to identify the possible existence of transitions and the atmospheric conditions under which they occur. The cold-to-warm (C2) and warm-to-cold (C3) simulations are used to study their reversibility.

3 Results

3.1 Description of the transitions and their reversibility

For the sake of clarity, this section focuses on the mean melt rate of Pine Island and Thwaites on the one hand, and of Crosson and Dotson ice shelves on the other hand. Cosgrove and Getz ice shelves undergo similar melt transitions, albeit with much lower and higher mean melt values, respectively (not shown).

For Pine Island–Thwaites, the heat flux perturbations lead to a permanent collapse of ice-shelf melting for air cooled by 2.5°C or more, with average melt rates below 0.3 m.w.e.yr^{-1} (meters of water equivalent per year, i.e., 1 m.w.e.yr^{-1} = 1000 kg.m^2.yr^{-1}), comparable to those experienced by the Ronne or Eastern Ross ice shelves (Rignot et al., 2013) (Fig. 4a). The -1°C perturbation leads to a collapse of melt rates after year 2000, while the -0.5°C perturbation keeps relatively high melt rates. Cycling our simulations by repeating the period 1958-2018 indicates that the cooler state over 2000-2018 is related to the forcing data and not to a slow drift of our regional system as melt rates are again high before 2000 in the repeated simulations (not shown). The heat flux perturbations associated with higher air temperatures lead to a limited increase in basal melt rates, with no more than a 34% increase for the +10°C perturbation. The effect of increasing air temperatures seems to saturate, with little differences between +2°C and +10°C warming. Basal melt rates beneath Crosson–Dotson show a similar behavior as Pine Island–Thwaites, with intermittent periods of very low melt rates for perturbations as small as -0.5°C, permanent collapse of melt rates below -2.5°C (melt rate is slightly higher than that of Pine Island–Thwaites with typical values of 0.8-1.0 m.w.e.yr^{-1}), and a 28% increase in melt rates for +10°C (Fig. 5a). It can also be noted that the amplitude of the seasonal melt cycle increases in response to warm perturbations for Pine Island–Thwaites but not for Crosson–Dotson.

The freshwater flux perturbations associated with lower precipitation lead to intermittent reductions in melt rates for precipitation reduced by 30% or more for Pine Island–Thwaites (Fig. 4b). Particularly low melt rates are found in the mid 1970s, early 2000s and late 2010s, but never reach the extremely low values resulting from the heat flux perturbations. This contrasts with Crosson–Dotson for which extended periods of very low melt rates (below 1.1 m.w.e.yr^{-1}) are found when precipitation is reduced by 20% or more (Fig. 5b). Increased precipitation does not have a strong effect on melt rates, with only 17% and 9% increase in response to doubled precipitation for Pine Island–Thwaites and Crosson–Dotson, respectively.

Finally, the momentum flux perturbations associated with northward-shifted wind at Pine Island–Thwaites results in intermittent decreases in melt rates, which is noticeable for a 2° northward wind shift (Fig. 4c). An extended collapse of basal melting is found over the period 2000-2018 for a northward wind shift of 4.7°. The extended period of low melt rates matches relatively well with those found for reduced precipitation. Crosson–Dotson is again more sensitive, with extended periods of very low melt rates for northward wind shift by 1° or more (Fig. 5c). The poleward-shifted winds lead to minor changes in basal melting: less than 5% and 15% increase for Pine Island–Thwaites and Crosson–Dotson, respectively.

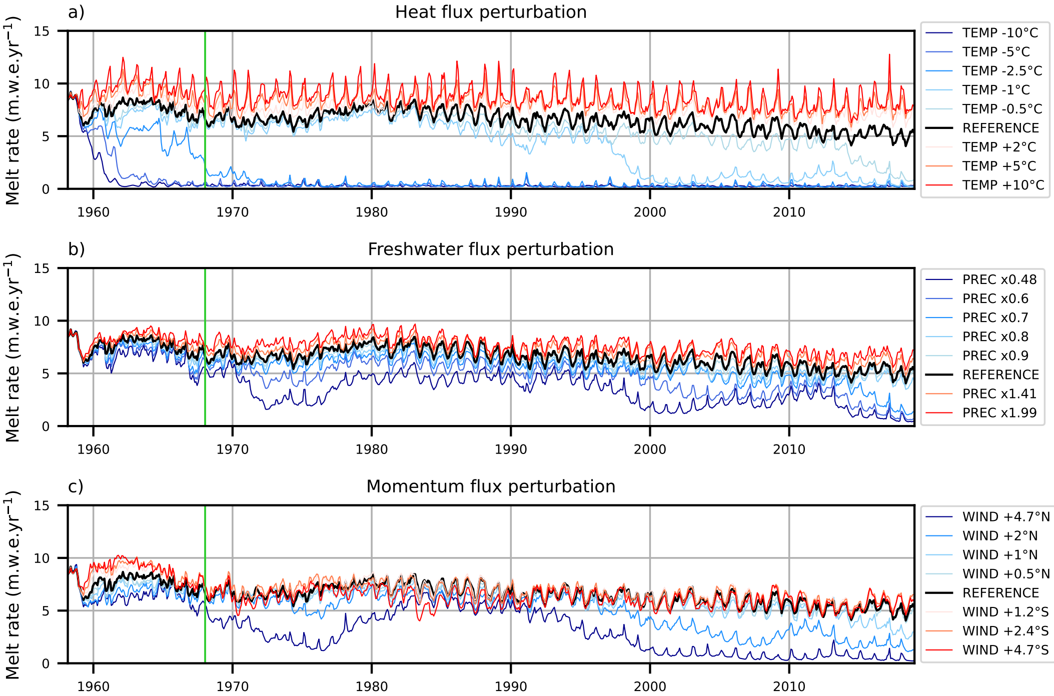

Figure 4. Evolution of monthly basal melting for Pine Island and Thwaites ice shelves over the period 1958-2018 for perturbations of (a) heat flux, (b) freshwater flux, and (c) momentum flux. The black curve (reference curve) corresponds to the simulation with the JRA55 reanalysis without modification. The red and blue curves correspond to simulations with atmospheric perturbations that aim to increase and decrease basal melting, respectively. The vertical green line indicates the end of the 10-year spin up.

We have just shown that abrupt transitions from a permanently high to a permanently low melt state can exist, and we now address the reversibility of these warm-to-cold transitions. We focus on transitions resulting from the strongest perturbations, i.e., air cooled by 10°C, precipitation decreased by 52%, and winds shifted northward by 4.7°, and we revert the atmospheric forcing to zero perturbation to re-run the period 1958-2018 starting from the 2018 perturbed state (Fig. 3). After 14 to 21 years, all perturbed melt time series go back to the unperturbed state and remain within ±5% of the original time series (Fig. 6). We conclude that all our warm-to-cold transitions in the Amundsen Sea are reversible. This also means that our description of the warm-to-cold transitions can be reverted to describe the cold-to-warm transitions.

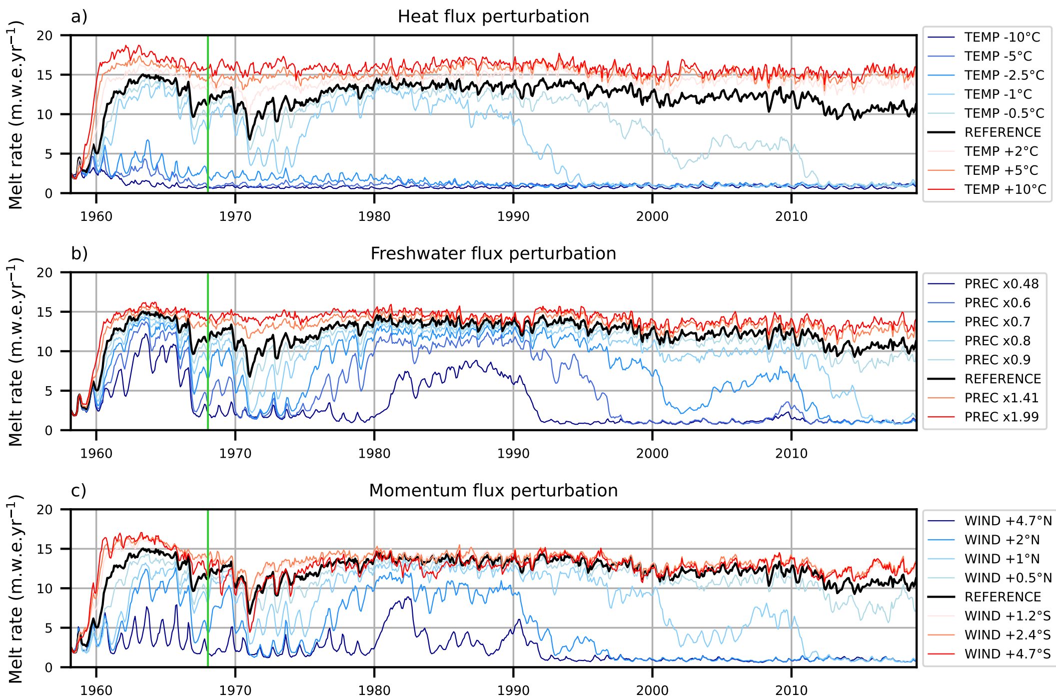

Figure 5. Evolution of monthly basal melting for Crosson and Dotson ice shelves over the period 1958-2018 for perturbations of (a) heat flux, (b) freshwater flux, and (c) momentum flux.. The black curve (reference curve) corresponds to the simulation with the JRA55 reanalysis without modification. The red and blue curves correspond to simulations with atmospheric perturbations that aim to increase and decrease basal melting, respectively. The vertical green line indicates the end of the 10-year spin-up.

We also evaluate the reversibility of cold-to-warm transitions, bearing in mind that such transitions may have occurred in the past. To do this, we take the final state of the 2nd cycle of 1958-2018 (unperturbed warm-climate (natural) forcing following a first cold-climate perturbed cycle), and we run a 3rd cycle of 1958-2018 again driven by the cold-climate perturbed forcing (Fig. 3). The two perturbed simulations (1st and 3rd cycle) converge (within ±5%) after 5-6 years for the perturbed heat flux, after 13-20 years for the perturbed freshwater flux and after 24-34 years for the perturbed momentum flux (Fig. 7). We conclude that the cold-to-warm transitions are also reversible in the Amundsen Sea.

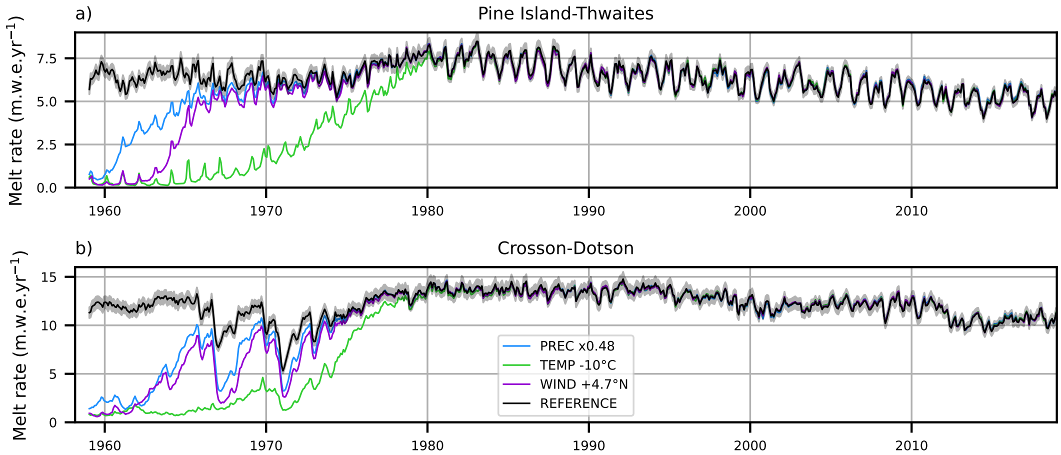

Figure 6. Evolution of the reversed warm-to-cold transition for (a) Pine Island and Thwaites ice shelves and (b) Crosson and Dotson ice shelves. Only the cold-climate perturbations of maximum amplitude are drawn. The black curve corresponds to the simulation driven by the JRA55 reanalysis without modification (natural state), with shading indicating ±5%.

3.2 Physical processes

From a general perspective, the main external drivers of ocean variations are (i) wind stress changes and (ii) surface heat and freshwater fluxes that modify the sea surface buoyancy (e.g., Marshall & Plumb, 2008; Talley et al., 2011). Winds induce a tangential stress at the ocean surface (directly or via sea-ice advection) and, thus, induce surface water transport towards the side of the wind. This transport results in areas of divergence and convergence that lead, respectively, to upwelling (Ekman suction) and downwelling (Ekman pumping). Surface heat and freshwater fluxes modify the sea surface buoyancy, which can affect convection and the horizontal circulation via density gradients. At high latitudes, the net sea-ice production plays a key role in these processes.

Here, we analyze the Ekman vertical velocity (w_{Ek}) and buoyancy flux at the ocean surface (B_s) to assess the impact of atmospheric forcing perturbations on the ocean properties. They are defined as:

$$w_{Ek} = \frac{1}{\rho_0} \vec{\nabla}_z \wedge \left(\frac{\vec{\tau}}{f} \right) \tag{1}$$

$$B_s = \frac{g\alpha}{c_p} Q + g\beta S_s F \tag{2}$$

where w_{Ek} is the upward Ekman vertical velocity, ρ_0 the reference seawater density, $\vec{\tau}$ the wind/sea-ice stress at the ocean surface and f the Coriolis parameter. B_s is the buoyancy flux at the ocean surface, c_p the specific heat, g the gravitational acceleration, S_s

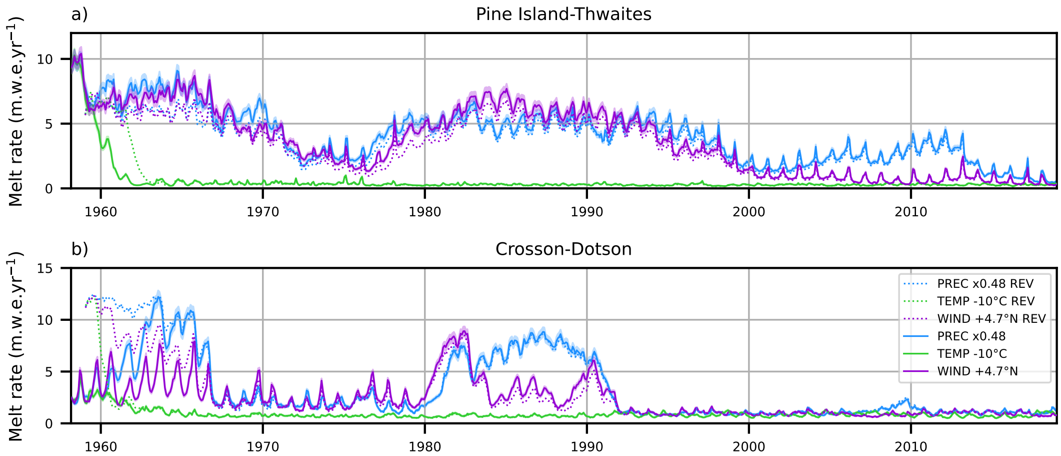

Figure 7. Evolution of the reversed cold-to-warm transition for (a) Pine Island and Thwaites ice shelves and (b) Crosson and Dotson ice shelves. Only the cold -climate perturbations of maximum amplitude are drawn. The solid line represents the melt rate after applying the cold-climate perturbations for the first time over 1958-2018 (1st cycle). The dotted line represents the melt rate under the cold-climate perturbations (3rd cycle) following a 1958-2018 cycle of unperturbed conditions (2nd cycle). The shading corresponds to the melt value of the perturbed state of the 1st cycle ±5%.

the sea surface salinity, α the surface thermal expansion coefficient of seawater and β the corresponding coefficient for salinity, F and Q are the heat and freshwater fluxes received by the ocean surface (positive downward).

A striking feature of our ensemble of experiments is that all types of perturbation approximately have the same ice-shelf melt evolution as a function of the surface buoyancy flux over the continental shelf (Fig. 8). The evolution curve consists of a highly sensitive regime bounded by a low plateau with no melt variations and a high plateau with lower melt sensitivity. The similarity between the three curves in Fig. 8 suggests that all perturbations mostly modify melt rates through changes of the surface buoyancy fluxes. Hereafter, we describe the processes that affect the surface buoyancy for the various types of perturbations.

The freshwater flux perturbations ("PREC" in Fig. 8) are the easiest to understand as precipitation directly affects the surface buoyancy. Lowering precipitation reduces the vertical density gradient and thereby favors convective mixing (Fig. 9c), which extracts the heat of the deep spreading CDW. A much colder water below the thermocline (Fig. 9a) explains the lower melt rates in the experiments with reduced precipitation. The opposite mechanism explains higher melt rates in the presence of enhanced precipitation. A small part of the freshwater flux modification is also related to minor changes in sea-ice production (Fig. 10a), due to the insulating properties of snow on sea ice (not shown).

The heat flux perturbations ("TEMP" in Fig. 8) have a less direct effect on surface buoyancy than just thermal expansion. Modified heat fluxes indeed explain less than 25% of the changes in surface buoyancy fluxes, while changes in freshwater fluxes related to net sea-ice production (i.e., growth minus melt) have a preponderant effect on the surface buoyancy fluxes. In the presence of colder air, the net sea-ice production increases considerably over the continental shelf (Fig. 10a), mostly due to a drastic decrease in summer melting (not shown). The case is very similar to decreased precipitation, albeit with a larger amplitude: increased convective mixing and related cooling below the thermo-

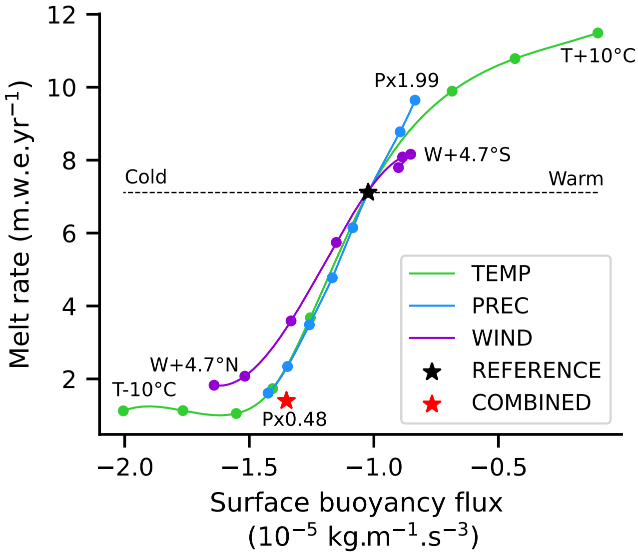

Figure 8. Mean ice-shelf melt rate in the Amundsen Sea as a function of the mean surface buoyancy flux over the Amundsen Sea continental shelf over the period 1988-2018. The green, blue and purple curves correspond to perturbations of heat, freshwater and momentum fluxes, respectively. The black star represents the reference case. The red star represents a more realistic case. It corresponds to the current climate - 0.5°C by combining the perturbation of all the fluxes (TEMP -0.5°C, PREC x0.96 and WIND +0.24°N).

cline (Fig. 9d,e,f) leads to reduced ice-shelf melting (Fig. 8). Its minimum is reached when the entire water column is close to the surface freezing temperature and the ice-shelf cavities are cold, i.e., melt rates are low and only controlled by the pressure dependency of the freezing point. For the warm perturbations, the opposite effect exists until there is too little net sea-ice production (Fig. 10a) to induce convective mixing. Beyond that, the CDW layer remains mostly unchanged and ice-shelf melt rates keep increasing only because warmer surface water gets in contact with the ice-shelf base (Fig. 9d,e,f). This is consistent with the aforementioned increased seasonality of the Pine Island and Thwaites melt rates (Fig. 4).

The results of the momentum flux perturbations are probably the most surprising as they affect the surface buoyancy fluxes (see "WIND" in Fig. 8), although we have been cautious not to modify the wind field in the calculation of the turbulent heat and evaporation fluxes. The impact of winds on sea-ice drift actually explains the variation in buoyancy flux. In the experiments with a northward wind shift, the net production increases (Fig. 10a) as winter sea-ice growth increases and summer melting decreases (not shown), but the sea-ice volume decreases (frozen area and thickness decrease in Fig. 10b,c). This is explained by enhanced advection of thinner sea ice towards the deep ocean (Fig. 11), which leaves space for more air-sea exchange on the continental shelf, i.e., more sea-ice production. Therefore, it is a similar perturbation of the vertical ocean stratification as in the case of the freshwater and heat perturbations. In the case of a southward wind shift, the annual sea-ice characteristics are little changed (Fig. 10) and so is the mean ice-shelf melt rate (Fig. 8).

Although surface buoyancy flux on the continental shelf appears as the major driver of ice-shelf basal melt changes, the set of curves in Fig. 8 do not exactly overlap, especially the curve associated with the momentum flux perturbation. For a given buoyancy flux, the cold-climate momentum perturbation induces a slightly higher melt rate than

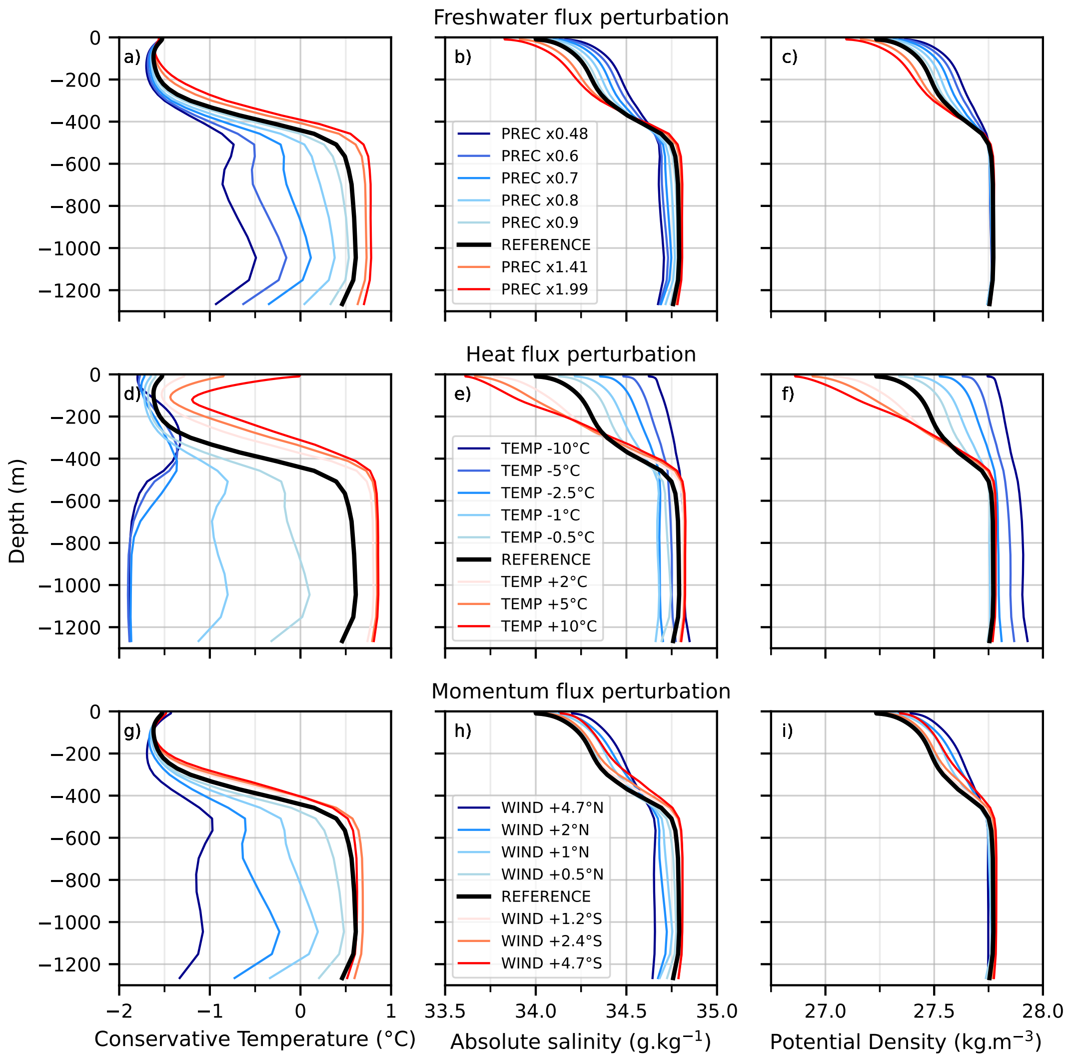

Figure 9. Shelf-averaged vertical profiles of conservative temperature (left), absolute salinity (middle) and potential density (right) over the period 1988-2018 for the various atmospheric perturbations : freshwater flux (top), heat flux (middle), and momentum flux (bottom) perturbations.

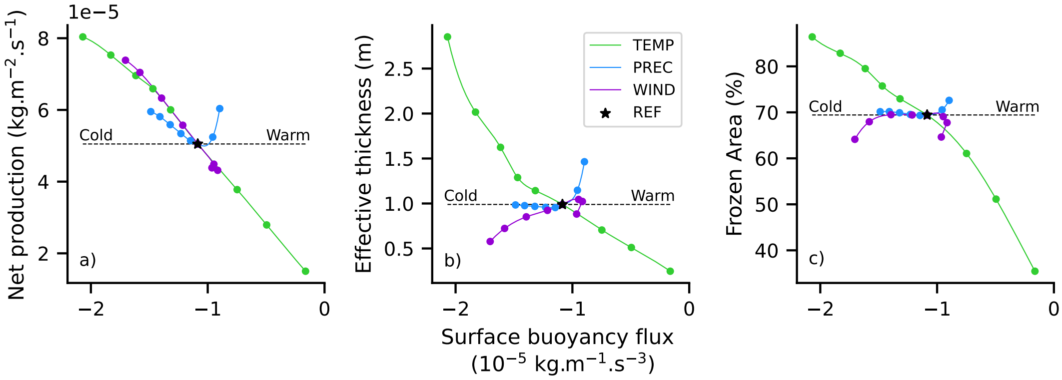

Figure 10. Sea-ice characteristics on the Amundsen Sea continental shelf related to surface buoyancy flux: (a) net production (i.e growth minus melt), (b) effective thickness (mean thickness over the whole continental shelf including ice-free areas), and (c) frozen area. The star represents the reference case. The perturbed flux configurations are colored in green for heat, blue for freshwater, and purple for momentum.

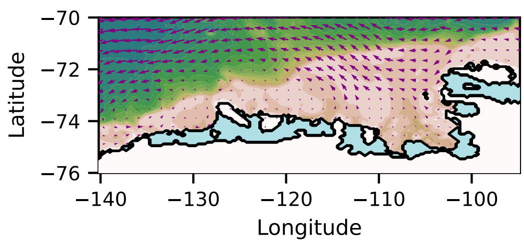

Figure 11. Sea-ice velocity anomaly relative to the reference case for a northward wind shift of 4.7°N. The background map is identical to the one shown in Fig. 1.

those related to freshwater and heat perturbations. The difference could be explained by Ekman dynamics if northward-shifted winds were associated with stronger Ekman upwelling, which would expose the ice shelves to a thicker layer of warm water (and, thus, partially inhibit the effects of decreased surface buoyancy fluxes). However, a stronger Ekman downwelling is found when considering the average velocity over the continental shelf (Fig. 13a).

A more detailed analysis at the ice-shelf scale shows that these differences are only noticeable for the eastern ice shelves (Fig. 12), i.e., for Cosgrove, Pine Island and Thwaites, suggesting regional differences in the acting mechanisms. We, therefore, analyzed the Ekman velocity at the entrance of the Pine Island–Thwaites Troughs as in Holland et al. (2019), but the most extreme point (+4.7°N) does not match either with the expected upwelling anomaly (Fig. 13b). Ekman pumping in our simulations is spatially very noisy (like Fig. 2a of Dotto et al., 2019), and we acknowledge a strong sensitivity to the exact location of the box used for the spatial average. Further investigation of Ekman velocities near individual ice-shelf fronts were similarly highly dependent on the location of box boundaries and therefore not conclusive. In summary, Ekman dynamics might explain the small difference in the melt response to the momentum perturbation and the other two perturbations, but such effect remains elusive. Other possible explanations may involve changes in ocean dynamics near the shelf break influencing the water mass properties advected onto the continental shelf.

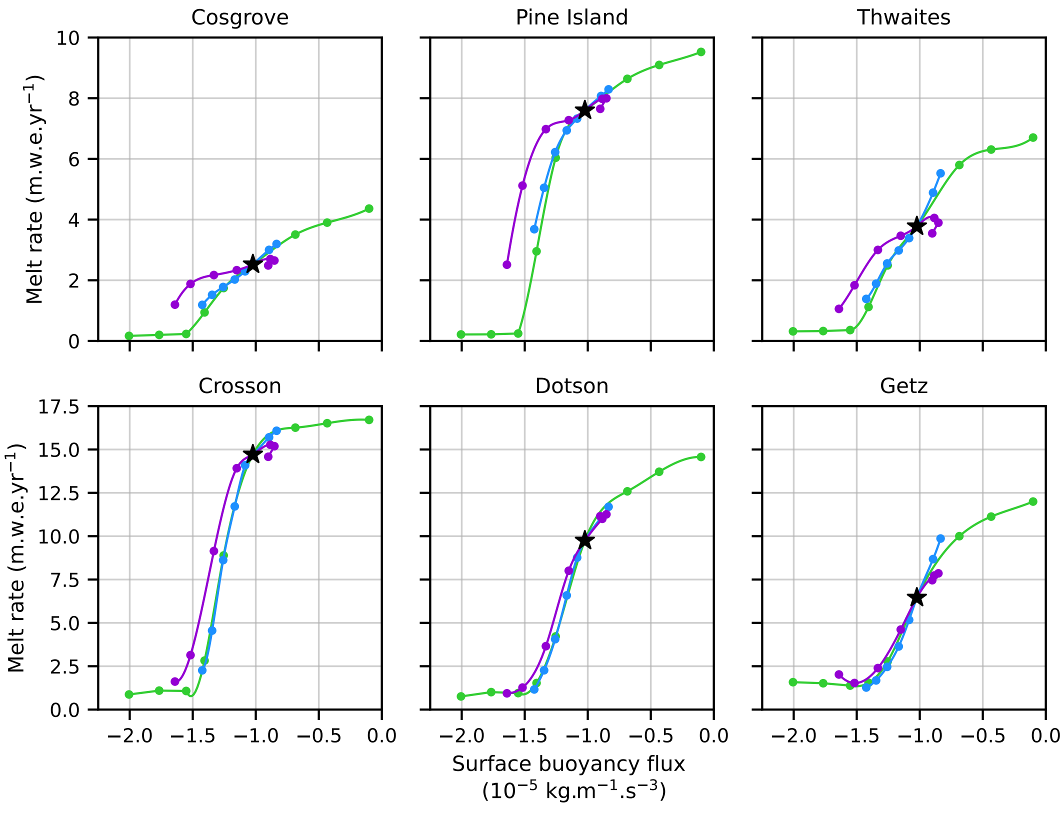

Figure 12. Mean basal melt rate of individual ice shelves in the Amundsen Sea as a function of the mean surface buoyancy flux over the Amundsen Sea continental shelf for the period 1988-2018. The green, blue and purple curves correspond to perturbations of heat, freshwater and momentum fluxes, respectively. The black star represents the reference case.

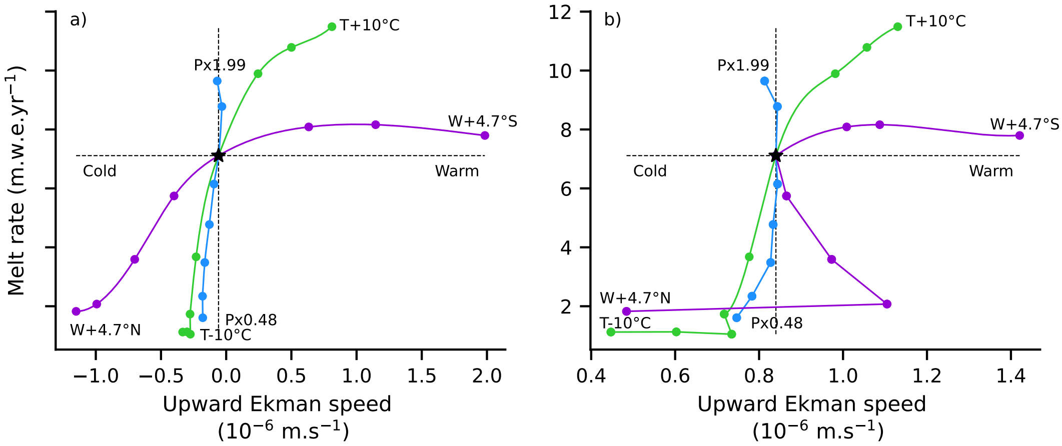

Figure 13. Mean basal melt rate as a function of upward Ekman velocity averaged over (a) the Amundsen Sea continental shelf and (b) over the entrance of Pine Island–Thwaites Troughs (box similar to the one defined in Fig. 1a of Holland et al. (2019)). The green, blue and purple curves correspond to perturbations of heat, freshwater and momentum fluxes, respectively. The black star represents the reference case.

4 Discussion and Conclusion

Robustness of the thresholds with respect to our model biases

Our regional model captures well the seasonal variability (see Section S3 in Supporting Information). Despite a calibration, however, the reference simulation still has a melt rate bias. The rate is outside the range of uncertainties of oceanic or satellite-based estimates, although of a similar order of magnitude to those found in other regional model studies (e.g., Nakayama et al., 2014; Kimura et al., 2017; Naughten et al., 2022), and has an overly low interannual variability (Figs. 4-5) compared to observational estimates (Dutrieux et al., 2014; Jenkins et al., 2018). Nevertheless, a more realistic interannual variability is observed for relatively small atmospheric perturbations. It should be kept in mind that a small perturbation of 0.5°C of the air temperature is of the order of magnitude of the reanalysis biases estimated by Jones et al. (2016) for the Amundsen Sea region. Biases are also large for precipitation, which is not constrained by data assimilation (Bromwich et al., 2011; Palerme et al., 2017). This means that the 'real' Amundsen Sea might correspond to a slightly cooler and drier climate than our reference state. However, the melt rate vs. buoyancy-flux curve is realistic and only the position of the reference state (black star) on this curve could be biased. Thus, the exact thresholds for air temperature, precipitation and wind shift for which a transition to the cold state occurs should still be considered as uncertain.

Robustness of the reversibility of abrupt transitions

Our results show that abrupt and reversible warm-to-cold as well as cold-to-warm transitions could occur in the Amundsen Sea for relatively weak regional atmospheric perturbations. The reversibility found in our experiments contrasts with the irreversibility of similar cold-to-warm transitions found in simulations of the Weddell Sea and Filchner-Ronne Ice-Shelf cavity (Hellmer et al., 2017; Hazel & Stewart, 2020; Comeau et al., 2022). The reason why the cold-to-warm transition is reversible in the Amundsen Sea but not in the Weddell Sea remains unclear. The melt-induced circulation was presented as the cause of the irreversibility in Hellmer et al. (2017), but the strong melt-induced circulation in the Amundsen Sea after a cold-to-warm transition (Jourdain et al., 2017; Donat-Magnin et al., 2017) does not seem able to maintain the onshore flow of Circumpolar Deep Water when the forcing is reverted to cold climate conditions. For the coldest perturbations, the deep Amundsen Sea is approximately at a conservative temperature of -1.9°C and an absolute salinity of 34.7 g kg^{-1} (Fig. 9d,e), i.e., typical of the High Salinity Shelf Water (HSSW) produced in the Weddell Sea. Hazel and Stewart (2020) explains the Weddell Sea tipping point by a feedback of ice-shelf meltwater to the salinity of newly formed HSSW. The tipping conditions and associated hysteresis may, therefore, be sensitive to the ratio between the HSSW formation rate and total ice-shelf basal mass loss, which could explain different regimes in the Weddell and Amundsen Seas.

These transitions and their reversibility may be complicated or facilitated by effects not taken into account in our simulations, such as the feedbacks with the large-scale atmospheric and oceanic circulations or the ice-sheet dynamics.

First of all, we do not change the ocean lateral boundary conditions in our sensitivity experiments, while the Amundsen Sea is also sensitive to changes of water properties advected from remote locations (Nakayama et al., 2018). It is known that large atmospheric changes over multiple decades will have global effects, and we, therefore, acknowledge that our regional point of view is somewhat limited. Furthermore, strong modifications of ice-shelf melting in the Amundsen Sea are expected to have significant consequences at circum-Antarctic (Nakayama et al., 2020) and global scales, with some positive feedback in which more meltwater enhances the stratification and further exposes ice shelves to CDW (Merino et al., 2018; Bronselaer et al., 2018; Golledge et al., 2019). Such feedback is not considered in our study and it is difficult to estimate how they would affect the thresholds and reversibility of our transitions.

Another limitation of our study is the missing evolution of ice-sheet dynamics in response to changes in ice-shelf melting. In the presence of higher melt rates, ice shelves are expected to thin and their grounding line to retreat. Ice-shelf thinning may slow down melting, if the ice draft raises above the thermocline (De Rydt et al., 2014). Conversely, strong grounding line retreat may enhance melting by exposing a larger basal area to warm water and thus favoring a stronger melt-induced sub-ice shelf circulation (Donat-Magnin et al., 2017). For some geometrical configurations, the retreat of the calving front may also favor melting by facilitating the circulation into ice-shelf cavities (Bradley et al., 2022). If ice-shelf basal melt rates increase sufficiently, the ice dynamics is likely to cross tipping points (Rosier et al., 2021), which would irreversibly put the Amundsen Sea in a different state due to the aforementioned feedback. Nonetheless, it is difficult to quantify the exact thresholds for which irreversibility would be found without using a fully coupled ocean–ice-sheet model.

Buoyancy vs wind-stress forcing

There is a consensus that the intrusion of warm CDW on the continental shelf plays a major role in the variability of ice-shelf basal melting, but several different processes have been suggested to explain their transport. As several studies independently investigate the eastern (Pine-Island–Thwaites) and western (Dotson–Getz) parts of the shelf (Wåhlin et al., 2012; Nakayama et al., 2013; Dotto et al., 2019) and as our study identifies distinct regimes between these two parts, it seems suitable to separate the analysis of processes according to these two regions.

Our study shows that the surface buoyancy flux on the shelf is the main driver of the multi-decadal changes in basal melting for the western Amundsen Sea (Dotson–Getz) regardless of perturbation. They also indicate no changes in local Ekman pumping in response to idealized wind perturbations, in contrast with the observational study by Kim et al. (2021), in which Ekman pumping along the Dotson–Getz trough explains 43% of the summer thermocline interannual variability. Dotto et al. (2020) have suggested that local winds at the shelf break may affect the eastward undercurrent and thereby the heat transport onto the continental shelf.

In the eastern Amundsen Sea (Cosgrove, Pine Island, Thwaites), our results again indicate that changes in the surface buoyancy fluxes are the main drivers of ice-shelf melt rate variations at multi-decadal time scales. A small deviation of the wind-perturbation experiments (Fig. 8 - purple line) nonetheless suggests that other wind-related processes might play a role, although the exact mechanism remains elusive. Previous studies have largely attributed interannual variability of the eastern Amundsen Sea to Ekman pumping at the shelf break (e.g., Holland et al., 2019; Dotto et al., 2019; Webber et al., 2019; Naughten et al., 2022), although sea-ice formation can also play a role in some specific years (St-Laurent et al., 2015; Webber et al., 2017).

In summary, changes in the surface buoyancy forcing appear to be the dominant driver of the variations in ice-shelf melting in all our experiments, whereas most previous studies have emphasized the direct role of wind stress, in particular through Ekman pumping. Part of the apparent discrepancy may be related to the multi-decadal time scale of our perturbations, which can slowly induce a change in the baroclinic balances that could overwhelm the relatively fast Ekman dynamics. We acknowledge, however, that our wind perturbations are highly idealized and may not capture the full complexity of wind changes at the continental shelf break, although we do have increasing Ekman velocities at the shelf break for the transition from cold to warm climate.

Implications for past and future climates

Our results indicate cold Amundsen Sea cavities (close to surface freezing point) for conditions of the Last Glacial Maximum (Fig. 8). This is consistent with grounding lines of paleo-ice streams near the continental shelf break during the last glacial period (Larter et al., 2014). Combined heat, freshwater and momentum perturbations maintained cold-cavities for climate conditions typical of -0.5°C compared to present day even in the presence of CDW at the continental shelf break (red star in Fig. 8). This suggests that pre-industrial conditions (approximately 1°C colder than present day (IPCC, 2021)) were associated with cold cavities in the Amundsen Sea. The transition to warm cavities may have occurred or be occurring as multi-year oscillations between cold and warm periods (Figs. 4-5). For conditions warmer than today, the decadal variability is relatively weak and cavities remain permanently warm. Our idealized experiments suggest a gradual but limited increase in ice-shelf basal melting in response to global warming beyond present levels.

Data and softwares

The model version and set of parameters used to run our experiments are provided in `https://github.com/Astrolabe-JC/Simulations_NEMO`. THE GITHUB REPOSITORIES WILL BE ARCHIVED ON `http://zenodo.org` AFTER ACCEPTANCE.

Acknowledgments

The authors would like to acknowledge Clara Burgard for her valuable advice on figures and presentations as well as Hélène Seroussi for her constructive feedback as a member of the PhD committee.

This study was funded by the European Union's Horizon 2020 research and innovation programme under grant agreements No 820575 (TiPACCs) and by the French National Research Agency under grant No ANR-19-CE01-0015 (EIS). This work was granted access to the HPC resources of CINES under the allocation A0100106035 attributed by GENCI.

References

Bett, D. T., Holland, P. R., Naveira Garabato, A. C., Jenkins, A., Dutrieux, P., Kimura, S., & Fleming, A. (2020). The impact of the Amundsen Sea freshwater balance on ocean melting of the West Antarctic Ice Sheet. *Journal of Geophysical Research: Oceans*, *125*(9), e2020JC016305.

Bradley, A. T., Bett, D. T., Dutrieux, P., De Rydt, J., & Holland, P. (2022). The influence of pine island ice shelf calving on melting.

Bromwich, D. H., Nicolas, J. P., & Monaghan, A. J. (2011). An Assessment of Precipitation Changes over Antarctica and the Southern Ocean since 1989 in Contemporary Global Reanalyses. *Journal of Climate*, *24*(16), 4189.

Bronselaer, B., Winton, M., Griffies, S. M., Hurlin, W. J., Rodgers, K. B., Sergienko, O. V., ... Russell, J. L. (2018). Change in future climate due to Antarctic meltwater. *Nature*, *564*(7734). doi: 10.1038/s41586-018-0712-z

Brovkin, V., Brook, E., Williams, J. W., Bathiany, S., Lenton, T. M., Barton, M., ... Yu, Z. (2021). Past abrupt changes, tipping points and cascading impacts in the Earth system. *Nature Geoscience*, *14*(8). doi: 10.1038/s41561-021-00790-5

Budge, J. S., & Long, D. G. (2018). A comprehensive database for Antarctic iceberg tracking using scatterometer data. *IEEE Journal of Selected Topics in Applied Earth Observations and Remote Sensing*, *11*(2), 434–442.

Carrère, L., Lyard, F., Cancet, M., Guillot, A., & Roblou, L. (2012). FES2012: A new global tidal model taking advantage of nearly twenty years of altimetry. In *Proceedings of the 20 years of progress in radar altimetry symposium (venice, italy)* (pp. 1–20).

Comeau, D., Asay-Davis, X. S., Begeman, C. B., Hoffman, M. J., Lin, W., Petersen, M. R., ... others (2022). The DOE E3SM v1. 2 Cryosphere Configuration: Description and Simulated Antarctic Ice-Shelf Basal Melting. *Journal of Advances in Modeling Earth Systems*, *14*(2), e2021MS002468.

Dekker, M. M., Von Der Heydt, A. S., & Dijkstra, H. A. (2018). Cascading transitions in the climate system. *Earth System Dynamics*, *9*(4). doi: 10.5194/esd-9-1243-2018

De Rydt, J., Holland, P. R., Dutrieux, P., & Jenkins, A. (2014). Geometric and oceanographic controls on melting beneath Pine Island Glacier. *Journal of Geophysical Research: Oceans*, *119*(4), 2420–2438.

Donat-Magnin, M., Jourdain, N. C., Kittel, C., Agosta, C., Amory, C., Gallée, H., ... Chekki, M. (2021). Future surface mass balance and surface melt in the Amundsen sector of the West Antarctic Ice Sheet. *Cryosphere*, *15*(2). doi: 10.5194/tc-15-571-2021

Donat-Magnin, M., Jourdain, N. C., Spence, P., Le Sommer, J., Gallée, H., & Durand, G. (2017). Ice-shelf melt response to changing winds and glacier dynamics in the amundsen sea sector, antarctica. *Journal of Geophysical Research: Oceans*, *122*(12), 10206–10224.

Dotto, T. S., Garabato, A. C., Bacon, S., Holland, P. R., Kimura, S., Firing, Y. L., ... Jenkins, A. (2019). Wind-driven processes controlling oceanic heat delivery to the amundsen sea, antarctica. *Journal of Physical Oceanography*, *49*(11). doi: 10.1175/JPO-D-19-0064.1

Dotto, T. S., Naveira Garabato, A. C., Wåhlin, A. K., Bacon, S., Holland, P. R., Kimura, S., ... Jenkins, A. (2020). Control of the Oceanic Heat Content of the Getz-Dotson Trough, Antarctica, by the Amundsen Sea Low. *Journal of Geophysical Research: Oceans*, *125*(8). doi: 10.1029/2020JC016113

Dutrieux, P., De Rydt, J., Jenkins, A., Holland, P. R., Ha, H. K., Lee, S. H., ... Schröder, M. (2014). Strong sensitivity of pine Island ice-shelf melting to climatic variability. *Science*, *343*(6167). doi: 10.1126/science.1244341

Favier, L., Durand, G., Cornford, S. L., Gudmundsson, G. H., Gagliardini, O., Gillet-Chaulet, F., ... Le Brocq, A. M. (2014). Retreat of Pine Island Glacier controlled by marine ice-sheet instability. *Nature Climate Change*, *4*(2). doi: 10.1038/nclimate2094

Garbe, J., Albrecht, T., Levermann, A., Donges, J. F., & Winkelmann, R. (2020). The hysteresis of the Antarctic Ice Sheet. *Nature*, *585*(7826). doi: 10.1038/s41586-020-2727-5

Garcia, H., Boyer, T., Baranova, O., Locarnini, R., Mishonov, A., Grodsky, A., ... Zweng, M. (2019). World Ocean Atlas 2018: Product Documentation.

Golledge, N. R., Keller, E. D., Gomez, N., Naughten, K. A., Bernales, J., Trusel, L. D., & Edwards, T. L. (2019). Global environmental consequences of twenty-first-century ice-sheet melt. *Nature*, *566*(7742), 65–72.

Gray, W. R., de Lavergne, C., Wills, R. C., Menviel, L., Spence, P., Holzer, M., ... Michel, E. (2021). Poleward shift in the southern hemisphere westerly winds synchronous with the deglacial rise in co2.

Griffies, S. M., Biastoch, A., Böning, C., Bryan, F., Danabasoglu, G., Chassignet, E. P., ... Yin, J. (2009). Coordinated Ocean-ice Reference Experiments (COREs). *Ocean Modelling*, *26*(1-2). doi: 10.1016/j.ocemod.2008.08.007

Gudmundsson, G. H. (2013). Ice-shelf buttressing and the stability of marine ice sheets. *Cryosphere*, *7*(2). doi: 10.5194/tc-7-647-2013

Hazel, J. E., & Stewart, A. L. (2020). Bistability of the Filchner-Ronne Ice Shelf Cavity Circulation and Basal Melt. *Journal of Geophysical Research: Oceans*, *125*(4), e2019JC015848.

Hellmer, H. H., Kauker, F., Timmermann, R., Determann, J., & Rae, J. (2012). *Twenty-first-century warming of a large Antarctic ice-shelf cavity by a redirected coastal current* (Vol. 485) (No. 7397). doi: 10.1038/nature11064

Hellmer, H. H., Kauker, F., Timmermann, R., & Hattermann, T. (2017). The fate of the Southern Weddell sea continental shelf in a warming climate. *Journal of Climate*, *30*(12). doi: 10.1175/JCLI-D-16-0420.1

Hinkel, J., Church, J. A., Gregory, J. M., Lambert, E., Le Cozannet, G., Lowe, J., ... van de Wal, R. (2019). Meeting User Needs for Sea Level Rise Information: A Decision Analysis Perspective. *Earth's Future*, *7*(3). doi: 10.1029/2018EF001071

Holland, P. R., Bracegirdle, T. J., Dutrieux, P., Jenkins, A., & Steig, E. J. (2019). West Antarctic ice loss influenced by internal climate variability and anthropogenic forcing. *Nature Geoscience*, *12*(9). doi: 10.1038/s41561-019-0420-9

IPCC. (2021). Climate Change 2021. *The Physical Science Basis. Contribution of Working Group 1 to Sixth Assessment Report of the Intergovernmental Panel on Climate Change*.

Jacobs, S., Hellmer, H. H., & Jenkins, A. (1996). Antarctic ice sheet melting in the southeast pacific. *Geophysical Research Letters*, *23*(9), 957–960.

Jacobs, S., Jenkins, A., Hellmer, H., Giulivi, C., Nitsche, F., Huber, B., & Guerrero, R. (2012). The Amundsen Sea and the Antarctic ice sheet. *Oceanography*, *25*(3). doi: 10.5670/oceanog.2012.90

Jenkins, A., Shoosmith, D., Dutrieux, P., Jacobs, S., Kim, T. W., Lee, S. H., ... Stammerjohn, S. (2018). West Antarctic Ice Sheet retreat in the Amundsen Sea driven by decadal oceanic variability. *Nature Geoscience*, *11*(10). doi: 10.1038/s41561-018-0207-4

Jones, R. W., Renfrew, I. A., Orr, A., Webber, B. G., Holland, D. M., & Lazzara, M. A. (2016). Evaluation of four global reanalysis products using in situ observations in the amundsen sea embayment, antarctica. *Journal of Geophysical Research*, *121*(11). doi: 10.1002/2015JD024680

Joughin, I., Smith, B. E., & Medley, B. (2014). Marine ice sheet collapse potentially under way for the thwaites glacier basin, West Antarctica. *Science*, *344*(6185). doi: 10.1126/science.1249055

Jourdain, N. C., Mathiot, P., Merino, N., Durand, G., Le Sommer, J., Spence, P., ... Madec, G. (2017). Ocean circulation and sea-ice thinning induced by melting ice shelves in the Amundsen Sea. *Journal of Geophysical Research: Oceans*, *122*(3). doi: 10.1002/2016JC012509

Jourdain, N. C., Molines, J. M., Le Sommer, J., Mathiot, P., Chanut, J., de Lavergne, C., & Madec, G. (2019). Simulating or prescribing the influence of tides on the Amundsen Sea ice shelves. *Ocean Modelling*, *133*. doi: 10.1016/j.ocemod.2018.11.001

Kim, T. W., Yang, H. W., Dutrieux, P., Wåhlin, A. K., Jenkins, A., Kim, Y. G., ... Cho, Y. K. (2021). Interannual Variation of Modified Circumpolar Deep Water in the Dotson-Getz Trough, West Antarctica. *Journal of Geophysical Research: Oceans*, *126*(12). doi: 10.1029/2021JC017491

Kimura, S., Jenkins, A., Regan, H., Holland, P. R., Assmann, K. M., Whitt, D. B., ... Dutrieux, P. (2017). Oceanographic controls on the variability of ice-shelf basal melting and circulation of glacial meltwater in the Amundsen Sea Embayment, Antarctica. *Journal of Geophysical Research: Oceans*, *122*(12), 10131–10155.

Large, W. G., & Yeager, S. G. (2004). *Diurnal to decadal global forcing for ocean and sea-ice models: The data sets and flux climatologies.* Citeseer.

Larter, R. D., Anderson, J. B., Graham, A. G., Gohl, K., Hillenbrand, C. D., Jakobsson, M., ... Spiegel, C. (2014). *Reconstruction of changes in the Amundsen Sea and Bellingshausen Sea sector of the West Antarctic Ice Sheet since the Last Glacial Maximum* (Vol. 100). doi: 10.1016/j.quascirev.2013.10.016

Lee, J.-Y., Marotzke, J., Bala, G., Cao, L., Corti, S., Dunne, J. P., ... others (2021). Future global climate: scenario-based projections and near-term information. IPCC.

Ligtenberg, S. R., van de Berg, W. J., van den Broeke, M. R., Rae, J. G., & van Meijgaard, E. (2013). Future surface mass balance of the Antarctic ice sheet and its influence on sea level change, simulated by a regional atmospheric climate model. *Climate Dynamics*, *41*(3-4). doi: 10.1007/s00382-013-1749-1

Lindsey, A. A. (1995). The exploration history of the Lindsey Islands, Antarctica, 1928-1994. In *Proceedings of the indiana academy of science* (Vol. 104, pp. 85–92).

Lyard, F., Lefevre, F., Letellier, T., & Francis, O. (2006). Modelling the global ocean tides: modern insights from fes2004. *Ocean dynamics*, *56*(5-6), 394–415.

Madec, G., & the NEMO Team. (2016). NEMO ocean engine. *Note du Pôle de modélisation*(27).

Marshall, J., & Plumb, R. A. (2008). *Atmosphere, Ocean, and Climate Dynamics.*

Masson-Delmotte, V., Stenni, B., Pol, K., Braconnot, P., Cattani, O., Falourd, S., ... Otto-Bliesner, B. (2010). EPICA Dome C record of glacial and interglacial intensities. *Quaternary Science Reviews*, *29*(1-2). doi: 10.1016/j.quascirev.2009.09.030

Mathiot, P., Jenkins, A., Harris, C., & Madec, G. (2017). Explicit representation and parametrised impacts of under ice shelf seas in the z*- coordinate ocean model NEMO 3.6. *Geoscientific Model Development*, *10*(7). doi: 10.5194/gmd-10-2849-2017

Matsuoka, K., Skoglund, A., Roth, G., de Pomereu, J., Griffiths, H., Headland, R., ... Melvær, Y. (2021). Quantarctica, an integrated mapping environment for Antarctica, the Southern Ocean, and sub-Antarctic islands. *Environmental Modelling and Software*, *140*. doi: 10.1016/j.envsoft.2021.105015

Mazur, A., Wåhlin, A. K., & Kreżel, A. (2017). An object-based SAR image iceberg detection algorithm applied to the Amundsen Sea. *Remote Sensing of Environment*, *189*, 67–83.

Merino, N., Jourdain, N. C., Le Sommer, J., Goosse, H., Mathiot, P., & Durand, G. (2018). Impact of increasing Antarctic glacial freshwater release on regional sea-ice cover in the Southern Ocean. *Ocean Modelling*, *121*, 76–89.

Merino, N., Le Sommer, J., Durand, G., Jourdain, N. C., Madec, G., Mathiot, P.,

& Tournadre, J. (2016). Antarctic icebergs melt over the Southern Ocean : Climatology and impact on sea ice. , *104*. doi: 10.1016/j.ocemod.2016.05.001

Morlighem, M., Rignot, E., Binder, T., Blankenship, D., Drews, R., Eagles, G., . . . Young, D. A. (2020). Deep glacial troughs and stabilizing ridges unveiled beneath the margins of the Antarctic ice sheet. *Nature Geoscience*, *13*(2). doi: 10.1038/s41561-019-0510-8

Nakayama, Y., Menemenlis, D., Zhang, H., Schodlok, M., & Rignot, E. (2018). Origin of Circumpolar Deep Water intruding onto the Amundsen and Bellingshausen Sea continental shelves. *Nature Communications*, *9*(1). doi: 10.1038/s41467-018-05813-1

Nakayama, Y., Schröder, M., & Hellmer, H. H. (2013). From circumpolar deep water to the glacial meltwater plume on the eastern amundsen shelf. *Deep Sea Research Part I: Oceanographic Research Papers*, *77*, 50–62.

Nakayama, Y., Timmermann, R., & H Hellmer, H. (2020). Impact of west antarctic ice shelf melting on southern ocean hydrography. *The Cryosphere*, *14*(7), 2205–2216.

Nakayama, Y., Timmermann, R., Schröder, M., & Hellmer, H. H. (2014). On the difficulty of modeling Circumpolar Deep Water intrusions onto the Amundsen Sea continental shelf. *Ocean Modelling*, *84*. doi: 10.1016/j.ocemod.2014.09.007

Naughten, K. A., Holland, P. R., Dutrieux, P., Kimura, S., Bett, D. T., & Jenkins, A. (2022). Simulated twentieth-century ocean warming in the amundsen sea, west antarctica. *Geophysical Research Letters*, e2021GL094566.

Palerme, C., Claud, C., Dufour, A., Genthon, C., Wood, N. B., & L'Ecuyer, T. (2017). Evaluation of Antarctic snowfall in global meteorological reanalyses. *Atmospheric Research*, *190*, 104–112.

Pattyn, F., Schoof, C., Perichon, L., Hindmarsh, R. C., Bueler, E., De Fleurian, B., . . . Vieli, A. (2012). Results of the marine ice sheet model intercomparison project, MISMIP. *Cryosphere*, *6*(3). doi: 10.5194/tc-6-573-2012

Rignot, E., Jacobs, S., Mouginot, J., & Scheuchl, B. (2013). Ice-shelf melting around antarctica. *Science*, *341*(6143). doi: 10.1126/science.1235798

Rosier, S. H., Reese, R., Donges, J. F., De Rydt, J., Hilmar Gudmundsson, G., & Winkelmann, R. (2021). The tipping points and early warning indicators for Pine Island Glacier, West Antarctica. *Cryosphere*, *15*(3). doi: 10.5194/tc-15-1501-2021

Rousset, C., Vancoppenolle, M., Madec, G., Fichefet, T., Flavoni, S., Barthélemy, A., . . . Vivier, F. (2015). The Louvain-La-Neuve sea ice model LIM3.6: Global and regional capabilities. *Geoscientific Model Development*, *8*(10). doi: 10.5194/gmd-8-2991-2015

Schoof, C. (2007). Marine ice-sheet dynamics. Part 1. The case of rapid sliding. *Journal of Fluid Mechanics*, *573*. doi: 10.1017/S0022112006003570

Smith, J. A., Andersen, T. J., Shortt, M., Gaffney, A. M., Truffer, M., Stanton, T. P., . . . Vaughan, D. G. (2017). Sub-ice-shelf sediments record history of twentieth-century retreat of Pine Island Glacier. *Nature*, *541*(7635). doi: 10.1038/nature20136

Spence, P., Griffies, S. M., England, M. H., Hogg, A. M. C., Saenko, O. A., & Jourdain, N. C. (2014). Rapid subsurface warming and circulation changes of Antarctic coastal waters by poleward shifting winds. *Geophysical Research Letters*, *41*(13). doi: 10.1002/2014GL060613

St-Laurent, P., Klinck, J., & Dinniman, M. (2015). Impact of local winter cooling on the melt of P ine I sland G lacier, A ntarctica. *Journal of Geophysical Research: Oceans*, *120*(10), 6718–6732.

Talley, L. D., Pickard, G. L., Emery, W. J., & Swift, J. H. (2011). *Descriptive physical oceanography: An introduction: Sixth edition.* doi: 10.1016/C2009-0-24322-4

Tsujino, H., Urakawa, S., Nakano, H., Small, R. J., Kim, W. M., Yeager, S. G., ... others (2018). JRA-55 based surface dataset for driving ocean–sea-ice models (JRA55-do). *Ocean Modelling*, *130*, 79–139.

Turney, C. S., Fogwill, C. J., Golledge, N. R., McKay, N. P., van Sebille, E., Jones, R. T., ... others (2020). Early last interglacial ocean warming drove substantial ice mass loss from antarctica. *Proceedings of the National Academy of Sciences*, *117*(8), 3996–4006.

Wåhlin, A. K., Muench, R. D., Arneborg, L., Björk, G., Ha, H. K., Lee, S. H., & Alsén, H. (2012). Some implications of ekman layer dynamics for cross-shelf exchange in the Amundsen sea. *Journal of Physical Oceanography*, *42*(9). doi: 10.1175/JPO-D-11-041.1

Webber, B. G., Heywood, K. J., Stevens, D. P., & Assmann, K. M. (2019). The impact of overturning and horizontal circulation in pine Island trough on ice shelf melt in the eastern Amundsen Sea. *Journal of Physical Oceanography*, *49*(1). doi: 10.1175/JPO-D-17-0213.1

Webber, B. G., Heywood, K. J., Stevens, D. P., Dutrieux, P., Abrahamsen, E. P., Jenkins, A., ... Kim, T. W. (2017). Mechanisms driving variability in the ocean forcing of Pine Island Glacier. *Nature Communications*, *8*. doi: 10.1038/ncomms14507

Wunderling, N., Donges, J. F., Kurths, J., & Winkelmann, R. (2021). Interacting tipping elements increase risk of climate domino effects under global warming. *Earth System Dynamics*, *12*(2). doi: 10.5194/esd-12-601-2021

Supporting Information for Drivers and reversibility of abrupt ocean state transitions in the Amundsen Sea, Antarctica

Justine Caillet[1], Nicolas C. Jourdain[1], Pierre Mathiot[1], Hartmut H. Hellmer[2], Jérémie Mouginot[1]

[1]Univ. Grenoble Alpes, CNRS, IRD, Grenoble INP, IGE, 38000 Grenoble, France

[2]Alfred Wegener Institute Helmholtz Centre for Polar and Marine Research, Bremerhaven, Germany

Contents of this file

1. Sections S1 to S6
2. Table S1
3. Figures S1 to S3

Introduction This supplementary document describes the calibration and evaluation of the reference simulation. It includes a description of both the observational data sets used to validate the configuration (see Section S1) and sensitivity experiments carried out in this study (see Section S2 and Table S1). The evaluation of these sensitivity experiments are made through the analysis of sea-ice extent (see Section S3 and Figure S1), temperature profiles (see Section S4 and Figure 2) and basal melt rates (see Section S5 and Figure S3).

S1. Observational Data Sets

The model is evaluated over the period 2012-2018 through a comparison with available observational datasets relative to sea-ice concentration, temperature profiles, and ice-shelves melt rates.

We used 1607 Conductivity-Temperature-Depth (CTD) profiles collected during summer campaigns from 1994 to 2018 (Dutrieux et al., 2014; Heywood et al., 2016) to evaluate the simulated temperature field. Individual CTD profiles are interpolated vertically onto the 75 vertical levels of our model configuration. The comparison to CTD data is performed by sampling model outputs in space (nearest profile) and time (linear interpolation between monthly outputs) following the actual CTD station distribution.

To evaluate the simulated sea-ice cover, the model outputs are compared to the NOAA/NSIDC Climate Data Record (CDR) of the Passive Microwave Sea-Ice Concentration dataset, version 4 (Meier et al., 2022), which provides daily and monthly estimates of sea-ice concentration in the polar regions for the period 1987-2020 on a 25 $\times$ 25 km stereographic grid. The observational data are interpolated onto the model grid and only concentration values above 0.15 are considered in both the model and observations due to observational uncertainties for lowest concentrations.

Finally, the simulated ice-shelf basal melt rates over the period 2012-2018 are compared to estimates based on satellite observations (Adusumilli et al., 2020).

S2. Sensitivity experiments

Preliminary to our main study, several sensitivity experiments were carried out in order to improve the fidelity of the model, in particular its ability to correctly represent ice-shelf basal melting. Their main characteristics are detailed in Tab. S1. In view of the shortcomings of the initial simulation (INITIAL), we explored three distinct ways to improve the representativeness of the model: (i) vertical mixing parameterization, (ii) forcing, and (iii) parameterization of melting under ice shelves.

The diffusivity and vertical turbulent viscosity coefficients are derived from a turbulent closure model that does not allow the thermocline depth to be represented correctly, particularly in the Southern Ocean (Rodgers et al., 2014). The thermocline depth is often too high in summer and when it is windy, as observed in INITIAL. To compensate for the lack of representation of some processes, an ad hoc parameterization exists in NEMO (see "TKE scheme" in Madec & the NEMO Team, 2016) to inject an amount D of additional turbulent kinetic energy below the mixed layer, with D defined as:

$$D = (1 - f_i)\, f_r e_s e^{-\frac{z}{h_\tau}} \tag{1}$$

where f_i is the sea-ice concentration, f_r the fraction of surface turbulent kinetic energy penetrating below the mixed layer, e_s the surface boundary condition of the turbulent kinetic energy (diagnosed by the TKE scheme), z the depth, and h_τ the vertical mixing length scale. To lower the depth of the thermocline, we modify the f_r parameter in EFR by taking the maximum value suggested by Madec (2008); Heuzé et al. (2015). In HTAU, we modify the vertical mixing length to $h_\tau = 60\,\mathrm{m}$, which is appropriate for high latitudes (Rodgers et al., 2014).

One of the main sources of divergence between our simulations and the observations is due to uncertainties in the forcing. We tested the model sensitivity to oceanic and atmospheric forcing. The BDY experiment includes the correction of oceanic lateral boundaries to match the World Ocean Atlas 2018 seasonal climatology (Garcia et al., 2019), and BDY + HTAU + FORCING takes into account another atmospheric reanalysis product, DFS5.2

(Dussin et al., 2016). The BDY + HTAU is a combination of the changes made both in BDY and HTAU.

Finally, in order to improve the basal melt rates, especially under Getz, Thwaites and Pine Island ice shelves, several corrections are explored. BDY + HTAU + GAMMA corrects basal melt rates through a modification of the heat and salt exchange coefficients (Γ_T and Γ_S, respectively). According to Jourdain et al. (2017), melt rates are proportional to $\Gamma^{1.25}$ where Γ is the heat/salinity exchange coefficient. Since melting under Getz was too high by about 1/3, the coefficients were multiplied by $\frac{2}{3}^{\frac{1}{1.25}}$ to reduce the melt rate by one third. The partial collapse of Thwaites Ice Shelf in 2015 altered the topography significantly. To assess the influence of topography on the melt rates under Thwaites Ice Shelf, the Rtopo2 topography (Schaffer et al., 2016) prior to the collapse of the ice shelf is used in BDY + HTAU + GAMMA + TOPO.

S3. Evaluation of sensitivity experiments: Sea-ice extent

The sea-ice cover analysis gives an insight into the seasonal variability (CTD profiles are collected only in austral summer and basal melt rates are often estimated over several years). In all our simulations, the seasonal variability is well represented (see Fig. S1) although the simulated summer and winter extrema differ from those in the NOAA/NSIDC climatology. Sea-ice extent is very sensitive to lateral boundary conditions. The correction of lateral boundaries to the World Ocean Atlas 2018 (BDY) results in an overestimation of the sea-ice extent (+35% in autral summer and +17% in winter), which hides an overestimation in the deep ocean and an underestimation in front of the ice shelves. The sea-ice extent is also sensitive to the stratification of the water column (HTAU). The change in vertical mixing leads to an underestimated sea-ice extent (-2% in austral summer -16%

in winter). The choice of atmospheric forcing impacts mostly the summer sea-ice cover, while changes in the vertical mixing parameter f_r, topography, and heat and salt exchange coefficients do not affect the sea-ice extent.

S4. Evaluation of sensitivity experiments: Temperature profiles

The CTD profiles measured in front of the Pine Island–Thwaites and Dotson–Getz ice shelves suggest a different flow pattern between the western and eastern continental shelf, consistent with Wåhlin et al. (2012); Dotto et al. (2019). The waters are generally 0.5°C warmer in the Pine Island–Thwaites area where CDW onshore flow is facilitated.

In front of the Pine Island–Thwaites ice shelves, INITIAL overestimates the subsurface temperature (0-400 m) by 1°C and the bottom temperature (800-1200 m) by 0.5°C, and the thermocline is too shallow by 200 m (Fig. S2). The ocean boundary correction with the World Ocean Atlas 2018 results in a significant change in the water column of the deep ocean. As the near-bottom temperature is essentially determined by the oceanic conditions at the shelf break, this correction lowers the temperature by about 0.5°C and thus approaches the observations in the lower part of the water column (deviation from observations less than 0.2°C below 600 m), although the thermocline is still too shallow. The increased vertical mixing length scale lowers the overestimated thermocline depth. Above 500 m, the temperature is lowered by an average of 0.5°C, but it is still higher than the CTD profiles (0.5°C on average). The other sensitivity tests have little impact on the temperature of the water column (0.2°C down to 300 m).

Concerning Dotson–Getz ice shelves, INITIAL overestimates the bottom temperature (800-1200 m) by 0.5°C, and the thermocline is again too shallow by 200 m (Fig. S2). The ocean boundary correction with the World Ocean Atlas 2018 lowers the temperature by about 0.5°C, resulting in a deviation from observations of less than 0.2°C. The increased vertical mixing length scale lowers the overestimated thermocline depth by 100 m, but has also an impact on near bottom temperature as does the change in the values of the heat and salt exchange coefficients.

S5. Evaluation of sensitivity experiments: Basal melt rates

We evaluate our basal melt rates by comparing them to satellite data estimates from Adusumilli et al. (2020) despite large uncertainties. Simulated cavity melt rates are close to published estimates for Venable, Abbot, and Cosgrove, underestimated for Pine Island and Thwaites (-30% and -77%, respectively for BDY + HTAU), although the vertical temperature distribution is overestimated by 0.5°C in front of these ice shelves, and overestimated for Crosson, Dotson and Getz (337%, 98% and 119%, respectively for BDY + HTAU) (see Fig. S3). In general, the interannual variation in melting is not as large as observed. Due to proportionality, a unique modification of the melt rates (BDY + HTAU + GAMMA) does not improve the overall results. Thus, we prefer to keep the original heat and salt exchange coefficients (Γ_T and Γ_S) in order to simulate correct melt rates for Pine Island rather than Getz ice shelf, which was already problematic when setting up Nemo's cavity module (Mathiot et al., 2017). The gain from the change in ice topography at Thwaites (BDY + HTAU + GAMMA + TOPO) is negligible.

S6. Conclusion on the sensitivity experiments

We selected the simulation (BDY + HTAU) as the reference simulation from which simulations with perturbations were built. The reference simulation captures well the seasonal variability with an average sea-ice extent error in austral summer and winter, of, respectively, 31% and 6%. The temperature between 700 and 1200 m depth is well represented on the shelf (deviation from observations less than 0.2°C). The thermocline is still too shallow, which corresponds to an overestimation of the temperature between 300 m and 600 m depth of about 0.5°C. Simulated basal melt rates are close to published estimates for Venable, Abbot and Cosgrove, underestimated for Pine Island and Thwaites (-30% and -77%, respectively), and overestimated for Crosson, Dotson and Getz (337%, 98% and 119%, respectively).

References

Adusumilli, S., Fricker, H. A., Medley, B., Padman, L., & Siegfried, M. R. (2020). Interannual variations in meltwater input to the Southern Ocean from Antarctic ice shelves. *Nature Geoscience*, *13*(9). doi: 10.1038/s41561-020-0616-z

Dotto, T. S., Garabato, A. C., Bacon, S., Holland, P. R., Kimura, S., Firing, Y. L., … Jenkins, A. (2019). Wind-driven processes controlling oceanic heat delivery to the amundsen sea, antarctica. *Journal of Physical Oceanography*, *49*(11). doi: 10.1175/JPO-D-19-0064.1

Dussin, R., Barnier, B., Brodeau, L., & Molines, J. M. (2016). The making of the drakkar forcing set dfs5. *DRAKKAR/MyOcean Rep*, *104*, 16.

Dutrieux, P., De Rydt, J., Jenkins, A., Holland, P. R., Ha, H. K., Lee, S. H., … Schröder, M. (2014). Strong sensitivity of pine Island ice-shelf melting to climatic variability. *Science*, *343*(6167). doi: 10.1126/science.1244341

Garcia, H., Boyer, T., Baranova, O., Locarnini, R., Mishonov, A., Grodsky, A., … Zweng, M. (2019). World Ocean Atlas 2018: Product Documentation.

Heuzé, C., Ridley, J. K., Calvert, D., Stevens, D. P., & Heywood, K. J. (2015). Increasing vertical mixing to reduce Southern Ocean deep convection in NEMO3.4. *Geoscientific*

Model Development, *8*(10). doi: 10.5194/gmd-8-3119-2015

Heywood, K. J., Biddle, L. C., Boehme, L., Dutrieux, P., Fedak, M., Jenkins, A., ... others (2016). Between the devil and the deep blue sea: The role of the Amundsen Sea continental shelf in exchanges between ocean and ice shelves. *Oceanography*, *29*(4), 118–129.

Jourdain, N. C., Mathiot, P., Merino, N., Durand, G., Le Sommer, J., Spence, P., ... Madec, G. (2017). Ocean circulation and sea-ice thinning induced by melting ice shelves in the Amundsen Sea. *Journal of Geophysical Research: Oceans*, *122*(3). doi: 10.1002/2016JC012509

Madec, G. (2008). Nemo ocean general circulation model reference manuel. *Paris: LODYC/IPSL.*

Madec, G., & the NEMO Team. (2016). NEMO ocean engine. *Note du Pôle de modélisation*(27).

Mathiot, P., Jenkins, A., Harris, C., & Madec, G. (2017). Explicit representation and parametrised impacts of under ice shelf seas in the z*- coordinate ocean model NEMO 3.6. *Geoscientific Model Development*, *10*(7). doi: 10.5194/gmd-10-2849-2017

Meier, W. N., Stewart, J. S., Windnagel, A., & Fetterer, F. M. (2022). Comparison of hemispheric and regional sea ice extent and area trends from noaa and nasa passive microwave-derived climate records. *Remote Sensing*, *14*(3), 619.

Rodgers, K. B., Aumont, O., Mikaloff Fletcher, S. E., Plancherel, Y., Bopp, L., De Boyer Montégut, C., ... Wanninkhof, R. (2014). Strong sensitivity of Southern Ocean carbon uptake and nutrient cycling to wind stirring. *Biogeosciences*, *11*(15). doi: 10.5194/bg-11-4077-2014

Schaffer, J., Timmermann, R., Erik Arndt, J., Savstrup Kristensen, S., Mayer, C., Morlighem, M., & Steinhage, D. (2016). A global, high-resolution data set of ice sheet topography, cavity geometry, and ocean bathymetry. *Earth System Science Data*, *8*(2). doi: 10.5194/essd-8-543-2016

Wåhlin, A. K., Muench, R. D., Arneborg, L., Björk, G., Ha, H. K., Lee, S. H., & Alsén, H. (2012). Some implications of ekman layer dynamics for cross-shelf exchange in the Amundsen sea. *Journal of Physical Oceanography*, *42*(9). doi: 10.1175/JPO-D-11-041.1

Table S1. Characteristics of sensitivity experiments used for model calibration (different terms are defined in section 1)

Simulation Name	f_r	h_τ	Boundaries	Γ_T	Γ_S	Topo	Forcing
INITIAL	0.05	$h_\tau\,(\phi)$	-	$2.21\,10^{-2}$	$6.19\,10^{-4}$	BedMachine	JRA55
EFR	0.10	$h_\tau\,(\phi)$	-	$2.21\,10^{-2}$	$6.19\,10^{-4}$	BedMachine	JRA55
BDY	0.05	$h_\tau\,(\phi)$	WOA18 Correction	$2.21\,10^{-2}$	$6.19\,10^{-4}$	BedMachine	JRA55
HTAU	0.05	$60\,m$	-	$2.21\,10^{-2}$	$6.19\,10^{-4}$	BedMachine	JRA55
BDY + HTAU	0.05	$60\,m$	WOA18 Correction	$2.21\,10^{-2}$	$6.19\,10^{-4}$	BedMachine	JRA55
BDY + HTAU + GAMMA	0.05	$60\,m$	WOA18 Correction	$1.60\,10^{-2}$	$4.48\,10^{-4}$	BedMachine	JRA55
BDY + HTAU + GAMMA + TOPO	0.05	$60\,m$	WOA18 Correction	$1.60\,10^{-2}$	$4.48\,10^{-4}$	RTopo2	JRA55
BDY + HTAU + FORCING	0.05	$60\,m$	WOA18 Correction	$2.21\,10^{-2}$	$6.19\,10^{-4}$	BedMachine	DFS5.2

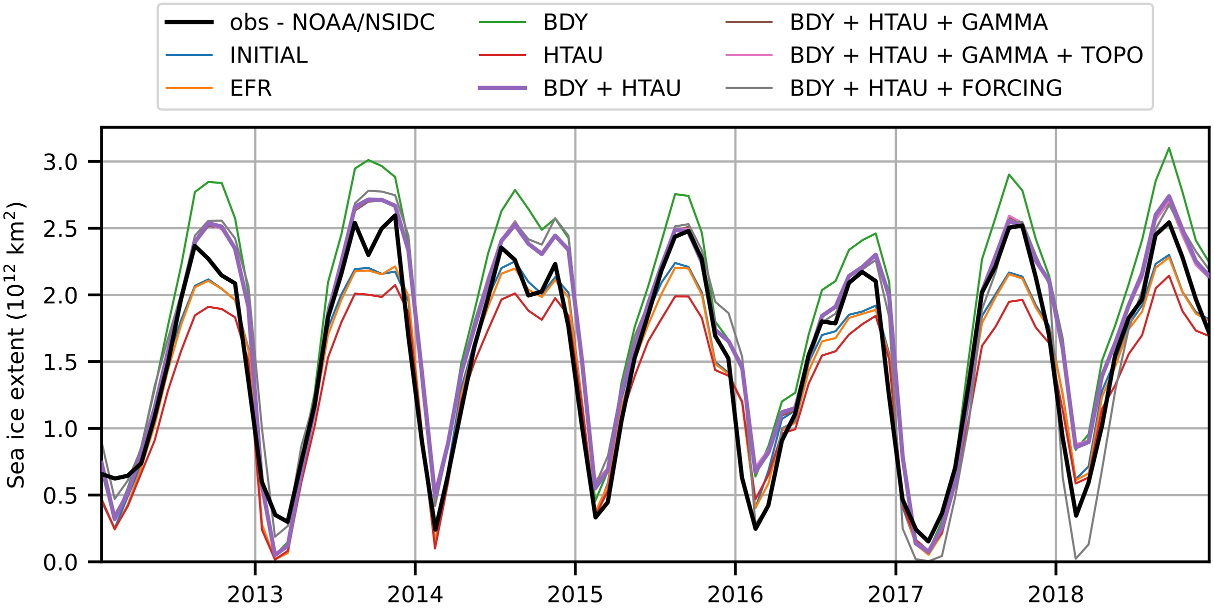

Figure S1. Variability of the sea-ice extent over the period 2012-2018 depending on the sensitivity experiments. As a reminder, only areas of sea-ice concentration greater than 0.15 were considered for the sea-ice extent estimation. The observations correspond to the NOAA/NSIDC Climate Data Record of Passive Microwave Sea-Ice Concentration dataset.

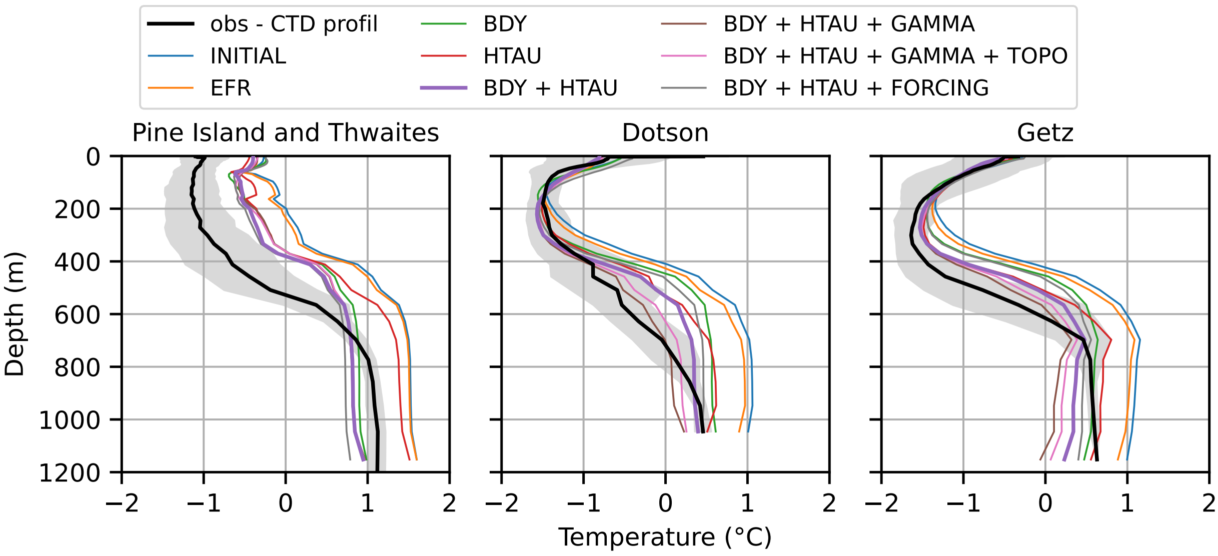

Figure S2. Mean conservative temperature profiles in front of Pine Island and Thwaites (left), Dotson(middle), and Getz (right) ice shelves depending on the sensitivity experiments. The observations are CTD profiles collected during austral summer campaigns from 2012-2018.

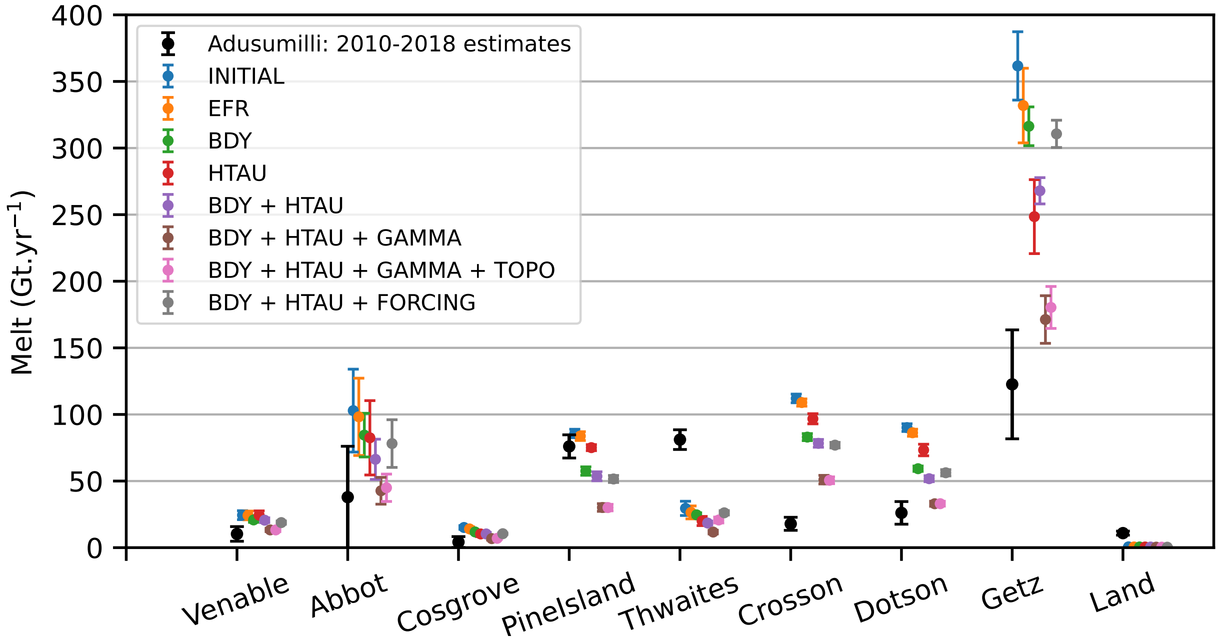

Figure S3. 2012-2018 mean basal mass loss under various Amundsen Sea ice shelves depending on the sensitivity experiments. Simulated basal mass losses are compared to the 2010-2018 estimates from Adusumilli et al. (2020)